



This is a repository copy of *Fire at high latitudes: Data-model comparisons and their consequences*.

White Rose Research Online URL for this paper:
<http://eprints.whiterose.ac.uk/86266/>

Version: Published Version

Article:

Kantzas, E., Lomas, M. and Quegan, S. (2013) Fire at high latitudes: Data-model comparisons and their consequences. *Global Biogeochemical Cycles*, 27 (3). 677 - 691. ISSN 0886-6236

<https://doi.org/10.1002/gbc.20059>

Reuse

Unless indicated otherwise, fulltext items are protected by copyright with all rights reserved. The copyright exception in section 29 of the Copyright, Designs and Patents Act 1988 allows the making of a single copy solely for the purpose of non-commercial research or private study within the limits of fair dealing. The publisher or other rights-holder may allow further reproduction and re-use of this version - refer to the White Rose Research Online record for this item. Where records identify the publisher as the copyright holder, users can verify any specific terms of use on the publisher's website.

Takedown

If you consider content in White Rose Research Online to be in breach of UK law, please notify us by emailing eprints@whiterose.ac.uk including the URL of the record and the reason for the withdrawal request.



eprints@whiterose.ac.uk
<https://eprints.whiterose.ac.uk/>

Fire at high latitudes: Data-model comparisons and their consequences

Euripides Kantzas,¹ Mark Lomas,² and Shaun Quegan¹

Received 12 June 2012; revised 8 May 2013; accepted 21 June 2013; published 9 August 2013.

[1] Fire is an endemic process at high latitudes, connected to a range of other land surface properties, such as land cover, biomass, and permafrost, and intimately linked to the carbon balance of the high-latitude land surface. Much of our current understanding of these links and their climate consequences is through land surface models, so it is important to ensure that for their credibility, these models should be consistent with available data. Over the vast panboreal region, a key source of information on fire is satellite data. Comparisons between satellite-based burned area data from the Global Fire Emissions Database and three dynamic vegetation models (LPJ-WM, CLM4CN, and SDGVM) indicate that all models fail to represent the observed spatial and temporal properties of the fire regime. Although the three dynamic vegetation models give comparable values of the boreal net biome production (NBP), fire emissions are found to differ by a factor 4 between the models, because of widely different estimates of burned area and because of different parameterizations of the fuel load and combustion process. Including a more realistic representation of the fire regime in the models shows that for northern high latitudes, (i) severe fire years do not coincide with source years or vice versa, (ii) the interannual variability of fire emissions does not significantly affect the interannual variability of NBP, and (iii) overall biomass values alter only slightly, but the spatial distribution of biomass exhibits changes. We also demonstrate that it is crucial to alter the current representations of fire occurrence and severity in land surface models if the links between permafrost and fire are to be captured, in particular, the dynamics of permafrost properties, such as active layer depth. This is especially important if models are to be used to predict the effects of a changing climate, because of the consequences of permafrost changes for greenhouse gas emissions, hydrology, and land cover.

Citation: Kantzas, E., M. Lomas, and S. Quegan (2013), Fire at high latitudes: Data-model comparisons and their consequences, *Global Biogeochem. Cycles*, 27, 677–691, doi:10.1002/gbc.20059.

1. Introduction

[2] Land masses at northern high latitudes, defined in this paper as poleward of 50°N and including the boreal and Arctic land masses, are characterized by huge expanses of boreal forest, wetlands, peatlands, and tundra lying on organic soils that account for 50% of the global belowground organic carbon [Tarnocai *et al.*, 2009]; northern peatlands alone hold a third of the global soil organic matter [Turetsky *et al.*, 2002]. Large parts are underlain by permafrost (continuous, widespread, or scattered). Low-average annual air temperatures have caused the rate of carbon

deposition to be on average higher than decomposition through the Holocene Era, leading to net accumulation of carbon; overall, these regions hold a third of the global terrestrial carbon [McGuire *et al.*, 1995]. Atmospheric inversion studies show that the high-latitude land surface continues to act as a carbon sink, estimated as $0.23 \pm 1.22 \text{ Pg C yr}^{-1}$ by Gurney *et al.* [2003], $0.19 \pm 0.53 \text{ Pg C yr}^{-1}$ by Baker *et al.* [2006], and $0.38 \pm 0.27 \text{ Pg C yr}^{-1}$ by Rödenbeck *et al.* [2003].

[3] Projections of the temperature response to climate show considerable warming of northern latitudes in the 21st century [Christensen *et al.*, 2007; Serreze and Francis, 2006]. Since 1900, the temperature in the Arctic has increased by 0.09°C per decade [Corell, 2005] and is projected to increase by 0.25–0.75°C per decade over the next 100 years, with associated increases in precipitation [Christensen *et al.*, 2007]. However, the effects of increased temperature on physical processes in the Arctic, the sensitivity of the carbon cycle to such changes, and the size of climate-carbon cycle feedbacks in this region remain highly uncertain [Friedlingstein *et al.*, 2006; McGuire *et al.*, 2009]. Such processes include the following: (a) decrease of snow cover and its effect on albedo and the radiation

¹Centre for Terrestrial Carbon Dynamics: National Centre for Earth Observation, University of Sheffield, Sheffield, UK.

²Department of Animal and Plant Sciences, University of Sheffield, Sheffield, UK.

Corresponding author: E. Kantzas, Centre for Terrestrial Carbon Dynamics: National Centre for Earth Observation, University of Sheffield, Hicks Bldg., Hounsfield Rd., Sheffield S37RH, UK. (e.kantzas@sheffield.ac.uk)

budget; (b) changes in the fire regime, with fire-resistant species benefiting from increased disturbance; (c) permafrost thawing and water table changes in peatlands with subsequent release of carbon and methane; and (d) increased photosynthesis with shrub and tree establishment at higher latitudes. For example, even though global circulation models driven by emissions scenarios show an increase in fire activity in boreal forests [Stocks *et al.*, 1998], analysis of the last 15 years of active fire data shows no statistically significant increase [Arino *et al.*, 2012]; however, the period examined is substantially smaller than the fire return interval at boreal latitudes, which usually exceeds 100 years [Kasischke *et al.*, 1995], so it does not allow a safe conclusion regarding trends.

[4] As pointed out by Cox and Stephenson [2007], during the first 10 years of a climate projection, the anthropogenic climate change signal is small compared to the decadal variability of climate, so over this period, the uncertainties in the projection originate mostly from the initial conditions used to describe the system, whereas at later times, they originate from errors in model formulation and uncertainties in the emission scenarios. A significant amount of work has been undertaken in recent years to address the initial value problem and to improve parameterizations by establishing a set of Essential Climate Variable data sets under the framework established by the Global Climate Observing System [GCOS, 2004, 2010]. This study focuses on fire-related Essential Climate Variables and processes at latitudes poleward of 50°N. To allow compact terminology, we will refer to this region as the boreal zone, even though it contains, for example, some temperate zones under maritime influence. In this region, fires provide a means to transfer large quantities of terrestrial carbon into the atmosphere with high spatial and temporal variability. Several studies using climate projections have hinted at a potential increase in burned area and length of the fire season in the boreal region [Flannigan and Vanwagner, 1991; Wotton and Flannigan, 1993] with an associated loss in stored carbon [Kasischke *et al.*, 1995], while on a global scale, increasing temperatures could act as a driver of the fire regime, leading to positive carbon feedbacks [Pechony and Shindell, 2010]. Nevertheless, fire dynamics are thought to be poorly represented in global climate models [Bowman *et al.*, 2009], as this paper clearly confirms for high northern latitudes. Marked differences are found between the properties of fires observed by satellites and their representations in three state-of-the-art land surface models, two of which are embedded in Intergovernmental Panel on Climate Change standard climate models. This raises important questions about the models and their ability to provide meaningful predictions under a changing climate:

[5] 1. Does the models' failure to capture the spatiotemporal variability in fire matter when estimating the effects of fire on high-latitude processes and quantities, such as net biome production (NBP), biomass, and the dynamics of permafrost?

[6] 2. Are there empirical data on the sizes of the carbon pools available as fuel in the boreal zone and their combustion completeness, and can these be used to test the models?

[7] 3. Can the models be reparameterized to conform better with observational data, and what are the consequences?

[8] These are addressed in the latter part of the paper.

2. Models, Data, and Methods

2.1. Description of Models

[9] Three dynamic vegetation models (DVMs) are used in this study, of which two, the Lund-Potsdam-Jena (LPJ) dynamic global vegetation model [Sitch *et al.*, 2003] and the Community Land Model 4 (CLM4) [Kloster *et al.*, 2010], are embedded in coupled climate models (the Bergen Climate Model [Tjiputra *et al.*, 2010] and the Norwegian Earth System Model, respectively). The third, the Sheffield Dynamic Global Vegetation Model (SDGVM), is a stand-alone terrestrial carbon-water model, chosen because of the ease with which it can be modified and used to test hypotheses within this study. Brief descriptions of these models are given below, focusing mainly on their relevance to studying carbon- and fire-related processes at high latitudes. Fuller descriptions are available in the references, and a detailed comparison of process representations in LPJ and SDGVM is given in Quegan *et al.* [2011].

[10] LPJ-WM [Wania *et al.*, 2009] is an enhanced version of LPJ tailored to high-latitude biomes, with adaptations to model peatland vegetation, peatland hydrology, and permafrost dynamics. It includes two new plant functional types (PFTs), flood-tolerant C3 graminoids and mosses: the latter represents the class of bryophytes, which have significant effects on the Arctic carbon balance [Street *et al.*, 2012]. For peatland hydrology, a new parameterization was introduced which considers the specific dynamics found in peat soils. To estimate permafrost behavior and permafrost active layer depth, soil temperature is calculated as a function of depth by numerically solving the one-dimensional heat diffusion equation using the Crank-Nicolson finite difference scheme in a column which incorporates snow, litter, and 12 soil layers, with an upper boundary condition given by the air temperature and a lower boundary condition of stable temperature. This required the hydrology module [Gerten *et al.*, 2004] to be modified to permit a greater number of soil layers.

[11] CLM4CN [Lawrence *et al.*, 2011] is an updated version of CLM4, the land component of the Community Earth System Model [Collins *et al.*, 2006], with a prognostic carbon-nitrogen biochemical model. CLM4CN has specific parameterizations for the thermal and hydraulic properties of organic soil [Lawrence and Slater, 2008] and incorporates boreal PFTs, and its soil temperature profiles and permafrost extent perform well when compared to observations [Lawrence *et al.*, 2008].

[12] The SDGVM [Woodward and Lomas, 2004; Woodward *et al.*, 1995] is one of the earliest of a host of DVMs which are now available. It has been used in several DVM comparison studies [Cramer *et al.*, 2001; Le Quere *et al.*, 2009; Piao *et al.*, 2009] and has proven to be a good indicator of the general trends produced by DVMs at global and regional scales. It contains no specific adaptations to high latitude conditions, e.g., it does not contain a permafrost module but is well suited to investigating the effects of land cover and some aspects of fire.

2.1.1. Fire Representation in Models

[13] Comparison of the three models is aided by the fact that they all follow similar approaches in producing fire emissions. The burned area in each grid cell is first calculated as a function of one or more climate variables, usually

temperature and moisture. It is then weighted against the available fuel in the grid cell, and finally, according to a model-specific set of rules that govern the combustion process, the fire emissions are calculated. A crucial observable quantity is therefore the burned area, which is derived in different ways between the models.

[14] In LPJ-WM, the probability of fire for a grid cell is calculated daily as a function of litter moisture, with temperature and available litter acting as limiting factors [Thonicke *et al.*, 2001]. By summing the daily probability over the course of the year, the annual length of the fire season is calculated, from which the annual fraction burned in each grid cell is estimated and distributed across the PFTs in proportion to the area they cover. CLM4CN incorporates the LPJ-WM algorithm to estimate the burned area [Kloster *et al.*, 2010] with modifications by Thornton *et al.* [2007] to accommodate the subdaily time step used by CLM and to adapt to the specifics of its variables, not all of which have exact equivalents in LPJ-WM. SDGVM produces burned area by an empirical model driven by monthly averages of temperature and precipitation and limits the fire return interval (FRI) to lie between 2 and 800 years, which in land surface process models is defined as the time required for successive fire events to cumulatively burn an area equal to the area of interest, usually a grid cell of a given spatial resolution. Hence, the FRI is equal to the reciprocal of the annual average fraction of area burned. None of the models incorporates fire propagation mechanisms within a grid cell or between neighboring grid cells; instead, as in most land surface models at such resolution, no lateral fluxes are included.

2.2. Fire and Climate Data

2.2.1. Satellite-Based Fire Products

[15] Three types of fire products are obtained from Earth Observation (EO) data: active fires, burned area, and fire radiative power. Active fire products, such as the Along Track Scanning Radiometer World Fire Atlas [Arino *et al.*, 2012] and the Moderate Resolution Imaging Spectroradiometer (MODIS) MOD/MYD14CMH product [Giglio, 2010], use the thermal channels of sensors to register anomalies of the surface temperature and thus identify hot spots. Burned area products, like the MODIS MCD45A1 (MODIS-BA) [Roy *et al.*, 2008] and the Global Fire Emissions Database-Burned Area (GFED-BA) [Giglio *et al.*, 2010], are derived by identifying reflectance changes in the visible channels of the sensor; GFED-BA also makes use of active fire products in its retrieval algorithm. Finally, Fire Radiative Power, as in the MODIS product MOD/MYD14CMH, is obtained from the thermal channels of a sensor and is a measure of the rate of radiant heat, which is related to the rate at which fuel is consumed [Wooster *et al.*, 2005].

[16] Both MODIS-BA and GFED-BA are examined in this study. MODIS-BA uses images acquired from the MODIS satellite series and calculates the date of burn for each 500 m pixel, from which burned area can be retrieved. Data are available for the years 2000–2011 but only for latitudes below 70°N. GFED-BA merges several types of EO data and products, of which the majority come from MODIS images, to create a global burned area data set at 0.5° resolution for the years 1996–2010; this is the same resolution as is used in all the models in this study.

[17] The GFED data set also contains estimates of carbon dioxide and other trace gas emissions from fire derived by a combination of satellite observations and modeling. Net primary production is first calculated from estimates of the fraction of available photosynthetically active radiation derived from EO data and allocated to plant types according to prescribed land cover. The Carnegie-Ames-Stanford Approach (CASA) biochemical model [Potter *et al.*, 1993] is then used to calculate the carbon pools (biomass, litter, etc.) in each 0.5° grid cell. Using the GFED burned area product, emissions for each carbon pool are then calculated as a function of monthly burned area, mortality, and combustion completeness, the last of which is calculated as a linear function of soil moisture. On a continental scale, the greatest uncertainties in carbon emissions are found in the boreal regions [van der Werf *et al.*, 2010].

[18] Although active fire products cannot be directly used in assessing model performance, they are important as they contribute to the GFED-BA burned area product. Fire Radiative Power has great potential for constraining models since it provides direct estimates of emissions from biomass burning [Roberts and Wooster, 2008], but no consistent data set for the boreal region yet exists, and hence, it is not used in this study.

2.2.2. Climate Data

[19] LPJ-WM and SDGVM were driven by the CRU TS 3.0 (Climate Research Unit Time Series) [Mitchell and Jones, 2005] (0.5° resolution, 1901–2006) and CLM4CN by the CRU + NCEP (National Centers for Environmental Prediction) climatology, based on CRU 2.0 and the NCEP reanalysis [Kanamitsu *et al.*, 2002], also at 0.5° resolution for the period 1949 to 2009. Before being driven by the complete climatology, the models undergo a spin-up phase, during which they are forced with a subset of the climate data set which cycles periodically until the carbon pools stabilize.

2.3. Modifying the Representation of Fire Statistics in Models

[20] The comparisons in section 3.2 demonstrate clearly that the spatial and temporal statistics of burned area produced by models are dramatically different from what is observed. To deal with this, we developed two approaches that introduce a stochastic element into the oversimplified representation of fire in the models, leading to greater consistency with the observed statistical properties of burned area. In the first, the temporal variability of burned area in SDGVM is forced to conform (in a statistical sense) with GFED-BA observations. In the second, LPJ-WM is modified to give more realistic spatiotemporal variability in burned area. These modifications are exploited in section 4.2, after the earlier sections of the paper make clear why they are needed.

2.3.1. Modifications to SDGVM

[21] The description of fire in SDGVM cannot be directly driven by GFED-BA data because, as in many DVMS, a spin-up (in this case, of 500 years) is required to bring the system to near-equilibrium before a transient run corresponding to current climate can take place; this needs a representation of the fire regime over the whole time period of the spin-up, together with the extra hundred years of the twentieth century. As a result, to investigate the extent to which the interannual variability observed in GFED-BA could affect SDGVM calculations, we assumed that the temporal

statistics of burned area observed at each location in GFED-BA are representative of the whole time period. To characterize this variability, the average annual fraction burned over the years 1997–2006 was first calculated for every grid cell, \mathbf{x} , to give the quantity

$$G(\mathbf{x}) = \sum_{i=1997}^{2006} G(\mathbf{x}, i), \quad (1)$$

where $G(\mathbf{x}, i)$ denotes the fraction of grid cell \mathbf{x} burned in year i in the GFED-BA data. Then the fluctuation of burned area about the mean at grid cell \mathbf{x} in year i was calculated by the scaling factor $SF(\mathbf{x}, i)$:

$$SF(\mathbf{x}, i) = G(\mathbf{x}, i)/G(\mathbf{x}). \quad (2)$$

[22] This yielded a map of scaling factors for year i . For each year of the SDGVM spin-up and the years preceding 1997, one of these 10 maps was randomly chosen, and at each grid cell, the fire probability was scaled by the corresponding map value. For the years 1997–2006 where data are available, the *observed* scale factors are used at each grid cell. In effect, the GFED-BA variance is added onto the (much smaller) variance that already occurs in the model. Note that the modification only adjusts the interannual variation, so the mean values and trends of burned area, emissions, and NBP are unaffected.

2.3.2. Modifications to LPJ-WM

[23] The LPJ-WM fire process was altered to yield a statistical distribution of burned area that closely resembles the GFED-BA data. This was achieved by deriving the cumulative distribution function (CDF) of the annual fraction burned per disturbed grid cell from GFED-BA and forcing LPJ-WM to obey the same distribution; this modified version of LPJ-WM will be denoted as LPJ-WMa. At the 0.5° resolution of GFED-BA, the CDF of annual fractional burned area per disturbed grid cell for boreal latitudes over the period 1997–2009 was found to be well approximated by a gamma distribution of the form

$$p(X \leq x) = \frac{1}{b^a \Gamma(a)} \int_0^x t^{a-1} e^{-t/b} dt \quad (3)$$

with parameters $a=0.21$ and $b=0.1$. Although the form of this distribution is determined by the GFED data, a constraint used to determine the parameters was that its mean value of 2.1% should be the same as for the original LPJ-WM; otherwise, fire would be completely decoupled from its process-based representation within the model. Note that the CDF will normally depend on the resolution of the data set used to produce it.

[24] For every grid cell in LPJ-WM, a random number, p , between 0 and 1 with probability defined by the CDF determines the fraction of the grid cell that will burn in the next fire. The timing of the fire event is fixed at each grid cell by aggregating the annual fraction of burn that would occur in the original model, but not allowing the fire to occur until the aggregate exceeds p . At this time, a fraction of the grid cell equal to the cumulative percentage is allowed to burn; the process is then reset and repeated. This procedure gives a temporal and spatial distribution of burned area in LPJ-WM that closely matches GFED observations while preserving the original mean burned area and can be readily adapted to other models.

3. Results

[25] In terms of climate feedbacks, the most important carbon quantity is the NBP, since this is the overall sink strength of the land surface. If lateral transport fluxes are ignored, the NBP contains three component fluxes:

$$\text{NBP} = \text{NPP} - R_h - D = \text{NEP} - D, \quad (4)$$

where NPP (net primary production) is the carbon available for plant growth from photosynthesis after autotrophic respiration has been subtracted, R_h is the heterotrophic respiration, $\text{NEP} = \text{NPP} - R_h$ is the net ecosystem production, and D is the disturbance flux, which we treat here as exclusively caused by fire even though other forms of disturbance can be included in CLM4CN. This allows a meaningful comparison with the available data sets, which only deal with burned area and fire emissions. However, in situ measurements indicate that other types of disturbance, for example insect damage and logging, cause significantly greater losses of carbon than fire over large parts of central Siberia [Quegan *et al.*, 2011].

3.1. Model-Based Estimates of Net Biome Production (NBP)

[26] All three models find the boreal region to be a net sink, as illustrated by Figure 1, which shows maps of average NBP over the period 1981–2006 estimated by the three DVMS, and Table 1, which gives the aggregated values for the panboreal region and for North America and Eurasia. LPJ-WM gives the largest values both overall and in each continent, being a factor of 1.5–2 larger than CLM4CN, while SDGVM takes intermediate values. Except for CLM4CN, the model estimates lie within the 300–600 Tg C yr⁻¹ range of estimates of the net uptake of CO₂ poleward of 45°N for the twentieth century found by a number of inventory studies [McGuire *et al.*, 2009].

[27] There are marked differences in spatial structure between the three models. LPJ-WM exhibits much higher spatial variability: 31% of its grid cells, distributed across all latitude bands, are sources, yielding average annual emissions of 118 Tg C yr⁻¹; these grid cells exhibit no special bias toward a particular PFT. For CLM4CN, 42.5% of the grid cells are weak sources, most of which occur at latitudes above 60°N, but these emit only 24.5 Tg C yr⁻¹, a factor of 5 less than LPJ-WM. SDGVM is quite different, exhibiting fairly homogeneous uptake across the panboreal region, with fewer than 5% of the grid cells acting as sources.

[28] All three models show an increasing trend in NBP over the period 1981–2006, with rates of increase given by 8.3 Tg C yr⁻² for LPJ-WM, 14.4 Tg C yr⁻² for SDGVM, and 3.4 Tg C yr⁻² for CLM4CN; however, only the SDGVM value is statistically significant. Atmospheric inversion studies reviewed by McGuire *et al.* [2009] find the interannual variability of NBP (defined as temporal standard deviation) for the Arctic land surface during the 1990s to have a value of up to ± 500 Tg C yr⁻¹, but for the same period, the models give lower values: ± 300 Tg C yr⁻¹ for LPJ-WM, ± 170 Tg C yr⁻¹ for SDGVM, and ± 153 Tg C yr⁻¹ for CLM4CN. The corresponding values for the period 1981–2006 are, respectively, ± 309 , ± 148 , and ± 143 Tg C yr⁻¹.

[29] The panboreal aggregate values of the components making up the NBP are shown in Figure 2. For all three models, the ratio of NPP to R_h is very similar, ranging from

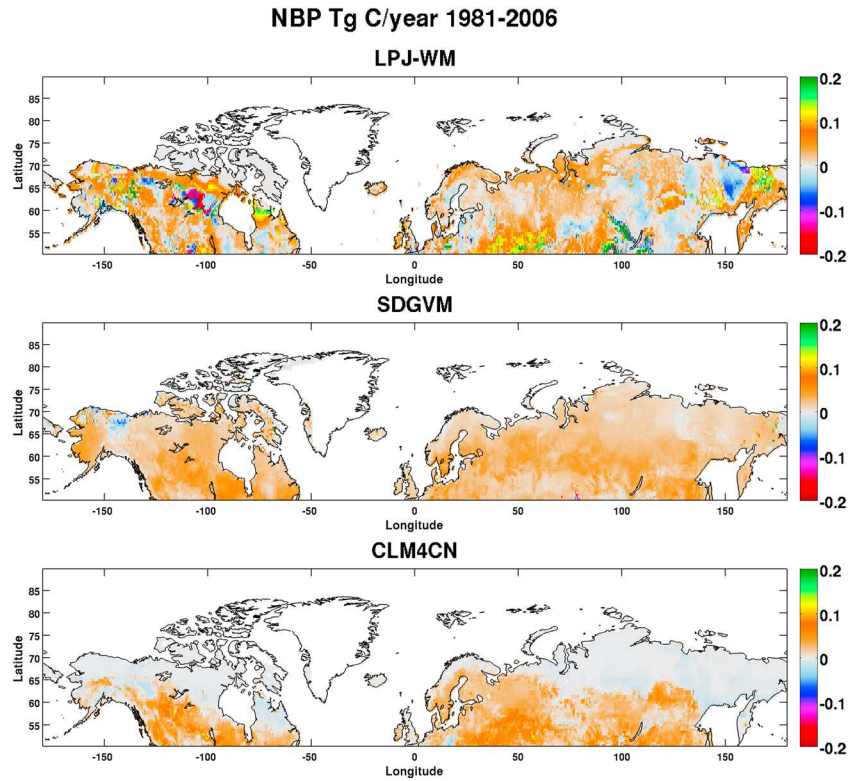


Figure 1. Annual NBP (in Tg C yr^{-1}) of the three models averaged over 1981–2006 for latitudes northward of 50°N .

1.08 to 1.10. LPJ-WM gives higher NEP ($1170 \text{ Tg C yr}^{-1}$) than both SDGVM (778 Tg C yr^{-1}) and CLM4CN (450 Tg C yr^{-1}), the last of which exhibits very low productivity for regions north of 65°N where the boreal shrub PFT is dominant. The large differences seen in NEP are compensated by large differences in emissions due to fire, which tend to equalize the NBP between the three models. Fire plays a particularly significant role in LPJ-WM, destroying on average around 57% of the NEP but only around 37% for CLM4CN and 35% for SDGVM. Hence, the ratio of fire emissions to NBP is much larger (1.30) for LPJ-WM than for SDGVM (0.62) and CLM4CN (0.58).

[30] In both Eurasia and North America, the emissions calculated by LPJ-WM are around a factor of 4 greater than those from CLM4CN and around 2–2.5 greater than from SDGVM (Figure 3 and Table 2). LPJ-WM also exhibits far greater spatial variability than the other two models, with significant fire fluxes at high latitudes in the Siberian Far East. In contrast, CLM4CN calculates no fire emissions north of 65°N , except for northern Scandinavia. SDGVM is similar to CLM4CN but with emissions extending to much higher latitudes.

Table 1. Annual NBP (in Tg C yr^{-1}) Averaged Over 1981–2006 for the Three Models Over North America, Eurasia, and All Northern High Latitudes

NBP (Tg C yr^{-1})	LPJ-WM	SDGVM	CLM4CN
North America	166	154	81
Eurasia	342	286	204
Boreal and Arctic	508	440	284

[31] Hence, for all models, fire is a very significant factor in determining the overall carbon balance and whether a given grid cell will act as a sink or a source (e.g., in LPJ-WM, 30% of the grid cells that are net sources were sinks before the fire emissions were subtracted). It is therefore important to establish whether measurements support the model estimates of fire emissions and the representation of the processes which give rise to them.

Carbon Balance gC , $50\text{--}75^\circ\text{N}$, 20-year average, Northern High Latitudes

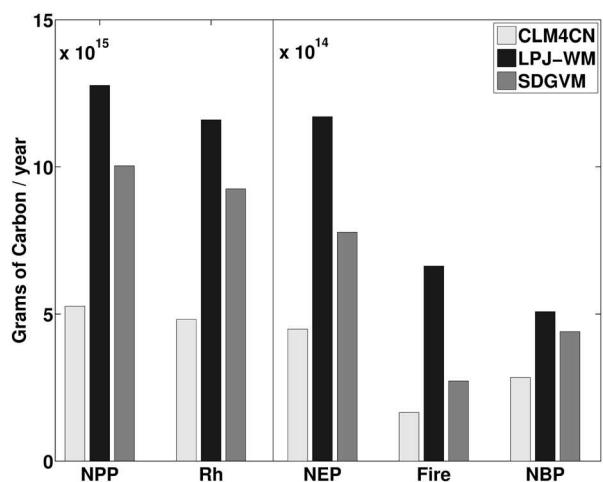


Figure 2. Northern high-latitude estimates of NPP, R_h , NEP, fire emissions, and NBP for the three models.

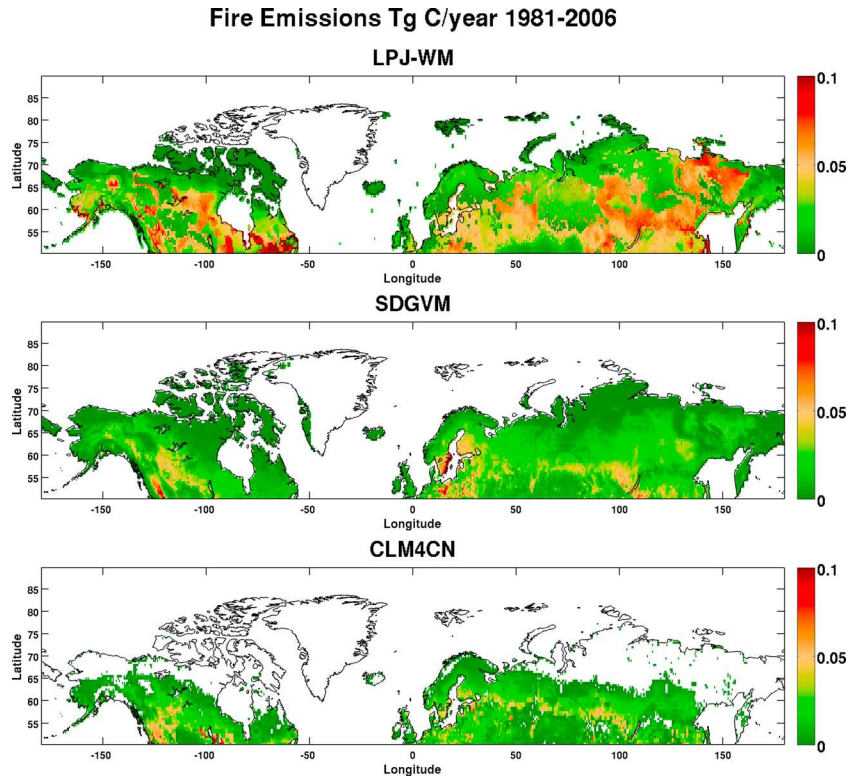


Figure 3. Annual fire emissions (in Tg C yr^{-1}) from northern high latitudes averaged over 1981–2006 for the three models.

3.2. Comparing Model Estimates of Burned Area With Satellite Observation: Observed and Modeled Spatial and Temporal Variability in Burned Area

[32] The annual average fraction of burned area per grid cell calculated over the period 1981–2006 by the three models is shown in Figure 4 (note the log scale) and summarized in Table 3, together with the equivalent results from the GFED-BA. With the exception of CLM4CN northward of 65° , every grid cell in all three models shows some degree of burn. In LPJ-WM and CLM4CN, this is fairly uniform and mostly less than 1%, while SDGVM exhibits more structure, with grid cells in southern Eurasia and the western US exhibiting average burned area up to 5%. The overall average annual burned area in SDGVM is 17.2 Mha yr^{-1} , which is around 60% more than LPJ and 100% more than CLM4CN.

[33] The observed panboreal burned area given by GFED-BA lies in the middle of the values from the three models but displays two major differences from the models:

[34] 1. The area burned in Eurasia is nearly 5 times greater than in North America according to GFED-BA, but the models all predict a value about 2 times greater.

[35] 2. GFED-BA exhibits much greater spatial variability than the models in the fraction of a grid cell that burns. Over the period 1997–2006, GFED-BA indicates that 80% of the area burned in the boreal zone originated from grid cells that experienced more than 10% burn and 50% from grid cells with more than 20% burn. In contrast, LPJ-WM and CLM4CN never exceed 2% burn, while 99.5% of the SDGVM grid cells are below 5%.

[36] Model-data differences become even clearer when individual years are considered, as illustrated by Figure 5,

which shows the burned areas in 2000 and 2002 over North America according to the three models and GFED-BA. The data indicate that 2002 was a much more severe fire year in North America than 2000, mainly because of the Long Creek Fire in Alaska and fires in Quebec, and the 2 years exhibit quite different spatial patterns, but these differences are not captured by the models. While burns occur in only a small proportion of GFED-BA grid cells each year, and large fractions of some cells are burned, in the models, a small fraction of almost every grid cell burns every year (except for most grid cells north of 65°N in CLM4CN, where fire is not permitted).

[37] This discrepancy arises because the treatment of fire in the models is deterministic, while in practice, fire is stochastic. For example, in Canada, large fires made up only 3% of the total fires occurring from 1959 to 1999 but contributed 97% of the burned area [Stocks *et al.*, 2002]. These rare events follow the law of small numbers, and their occurrence

Table 2. Annual Carbon Emissions (Tg C yr^{-1}) Averaged Over 1981–2006 for the Three Models Over North America, Eurasia, and All Northern High Latitudes^a

Fire Emissions (Tg C yr^{-1})	LPJ-WM	SDGVM	CLM4CN	GFED
North America	192	71	55	56
Eurasia	471	201	110	144
Boreal and Arctic	663	272	164	200

^aAlso shown are the emissions from GFED averaged over 1997–2009 for the same regions.

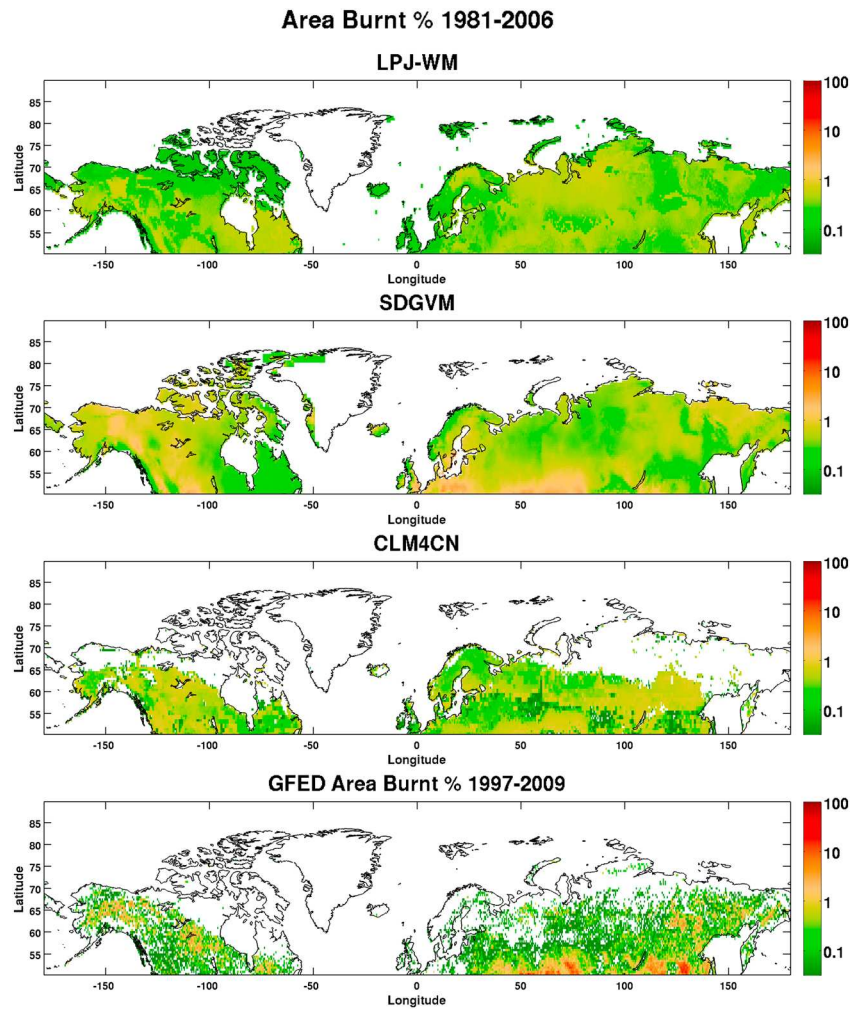


Figure 4. Percentage of annually burned area in logarithmic scale at northern high latitudes averaged over 1981–2006 for the three models and over 1997–2009 for GFED-BA.

is usually modeled by a Poisson distribution [Jiang *et al.*, 2012; Mandallaz and Ye, 1997]. The lack of such a random component in fire occurrence is not apparent when FRI or annual average burn is used to compare model outputs with data.

[38] The total burned areas of the panboreal region, North America, and Eurasia estimated by GFED-BA for 1997–2006, MODIS-BA for 2002–2006, and the three models for 1981–2006 are compared in Figure 6 (left). Since GFED-BA exploits MODIS-BA, these two observational data sets correlate well over their common time period from 2002 to 2009, though MODIS-BA produces more burned area in Eurasia and less in North America [Giglio *et al.*, 2010; van der Werf *et al.*, 2010]. In contrast, none of the models shows any significant correlation with GFED-BA for the overlapping period 1997–2006, either by continent or globally, as has previously been noted for CLM4CN over the panboreal region [Kloster *et al.*, 2010]. The observations also exhibit markedly greater interannual variability than the model values, especially LPJ-WM and CLM4CN. Hence, the mean values of the four estimates shown in Table 3 do not really capture the model-data differences; for example, the global mean burned area in GFED-BA lies between the values from the three models, but values in some individual years are high and close to those from SDGVM, while other

years give much lower values that are closer to those from the other two models. CLM4CN and LPJ-WM produce similar burned areas, with those from LPJ-WM always being higher, while SDGVM consistently produces values that are 50–100% larger, globally and in each continent.

3.3. Estimated Fire Emissions

[39] Comparisons between the four time series of burned area and emissions for GFED and the three models exhibit two striking differences (Figure 6):

[40] 1. Despite LPJ-WM producing burned area that is comparable with CLM4CN and much less than SDGVM,

Table 3. Annual Burned Area (in Mha yr^{-1}) Averaged Over 1981–2006 for the Three Models Over North America, Eurasia, and All Northern High Latitudes^a

Burned Area (Mha yr^{-1})	LPJ-WM	SDGVM	CLM4CN	GFED-BA
North America	3.4	5.4	2.9	2.04
Eurasia	7.2	11.8	5.8	10.0
Boreal and Arctic	10.6	17.2	8.7	12.04

^a Also shown is the burned area from GFED-BA averaged over 1997–2009 for the same regions.

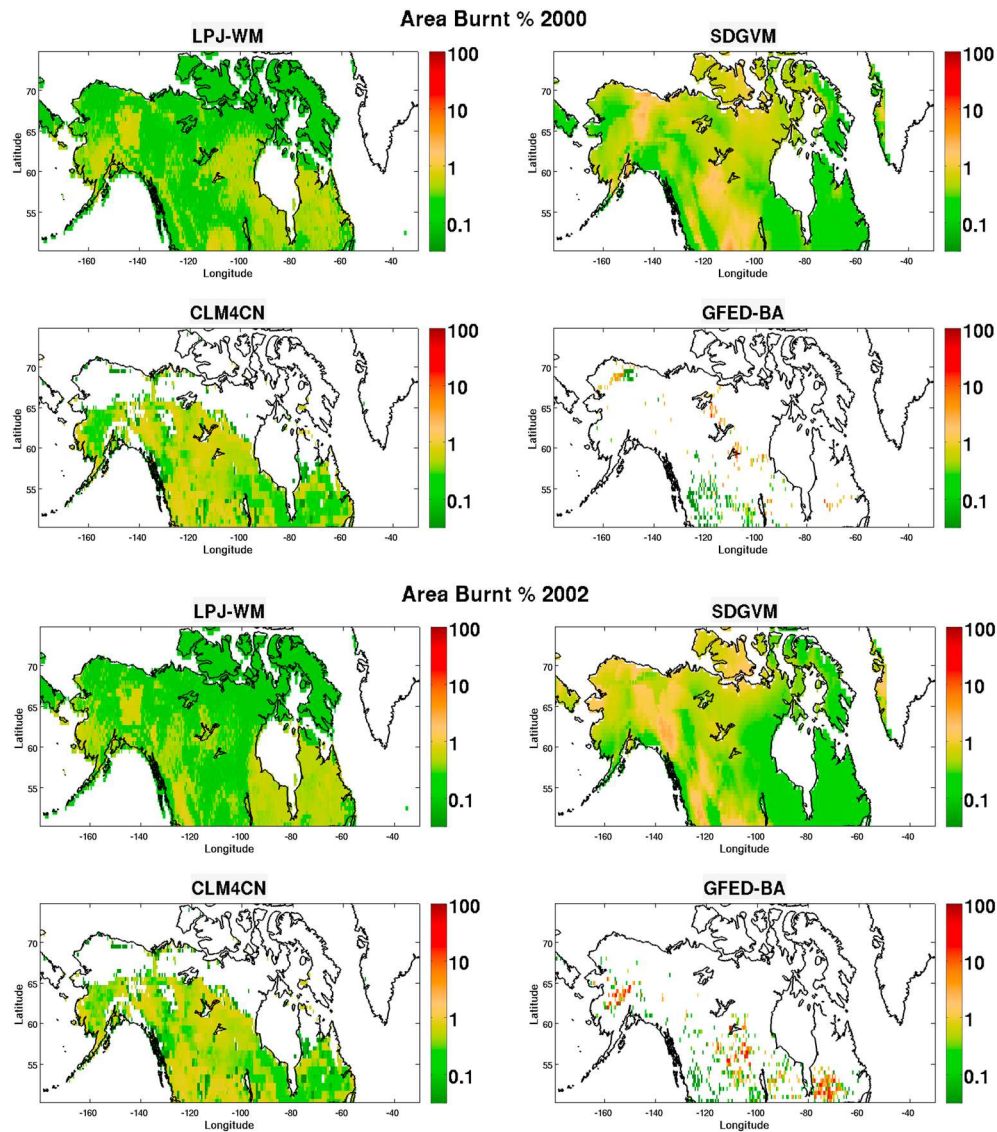


Figure 5. Percentage of burned area in logarithmic scale in 2000 and 2002 over North America for the three models and GFED-BA.

its estimates of emissions are higher than those from the other two models by a factor 2 or greater, both globally and in each continent.

[41] 2. Although SDGVM gives much greater burned area than either of the other models, its emission estimates are comparable to those of CLM4CN in North America and only about 30% higher than those of CLM4CN in Siberia.

[42] It should be noted that although the burned area in GFED is derived from observations, GFED *emissions* are calculated using the CASA model; hence, all four emission estimates in Figure 6 are model based. It can also be seen that the mean emissions from GFED, CLM4CN, and SDGVM are comparable, but LPJ-WM gives a much higher value (Table 2).

[43] The relation between burned area and emissions is a function of available fuel (biomass, litter, and carbonaceous soils) and the effectiveness with which fires consume this fuel, so it can be relatively complex at the local scale. However, at continental scales, a fairly simple picture emerges, as can be seen from Figure 7, which plots emissions

against burned area in North America and Eurasia for each year from 1981 to 2006 for the three models and emissions from GFED against burned area from GFED-BA for 1997–2009. A best linear fit to each plot is also shown, whose slope gives the mean emissions per unit area burned, and is a function of combustion completeness and the fuel load available in each model.

[44] Sharp differences in fire emissions are seen between all four estimates. Apart from CLM4CN, annual emissions are almost linearly related to burned area. The emissions per unit burned area are much higher for LPJ-WM than for the other models and larger for GFED than SDGVM in both North America and in Eurasia, while the R^2 value for CLM4CN is too low to assign any useful meaning to the calculated slope. All the estimates indicate that fires in North America produce more emissions per unit area than in Eurasia; this agrees with studies by *Wooster and Zhang* [2004], based on measurements of Fire Radiative Power, and has been attributed to the predominance of crown or canopy fires in North America, while crawling or surface fires tend to

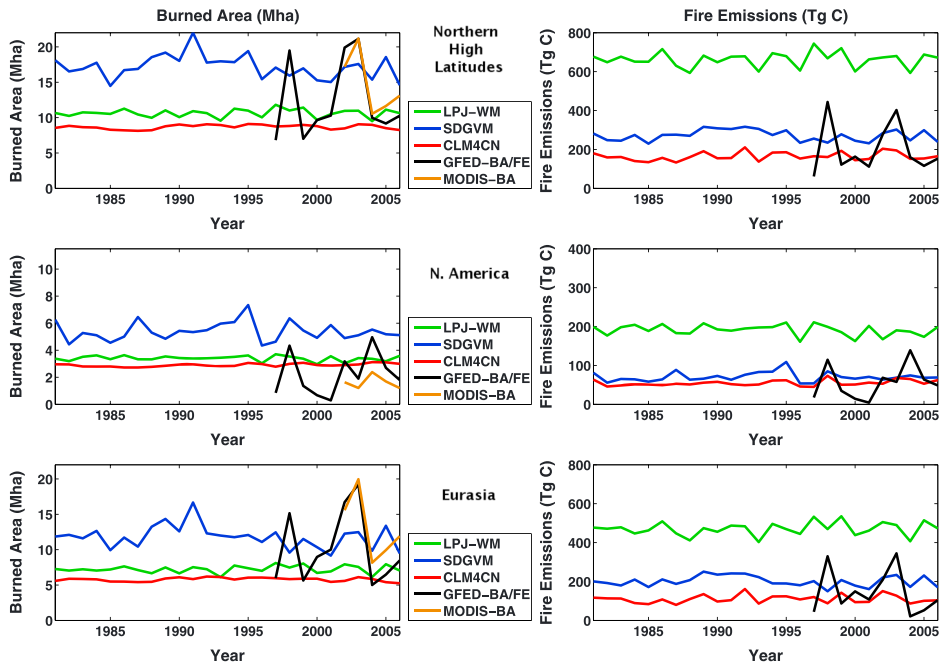


Figure 6. (left) Total area burned per year (Mha yr^{-1}) for the northern high latitudes, North America, and Eurasia as calculated by the three models and given by GFED-BA and MODIS-BA. (right) The corresponding fire emissions (Tg C yr^{-1}) for the models and GFED.

dominate in Eurasia. With the exception of CLM4CN, the R^2 values are very high in North America but smaller in Eurasia; this may be because many fires in Eurasia occur at latitudes from 50°N to 65°N (Figure 4), where, even though herbaceous and tree cover are equally present overall, they are highly

clustered, with herbaceous cover dominating the western part and forests the eastern. The difference in biomass between the two types causes a partial decoupling of burned area and fire emissions, a phenomenon which is also observed at global scale [van der Werf *et al.*, 2006].

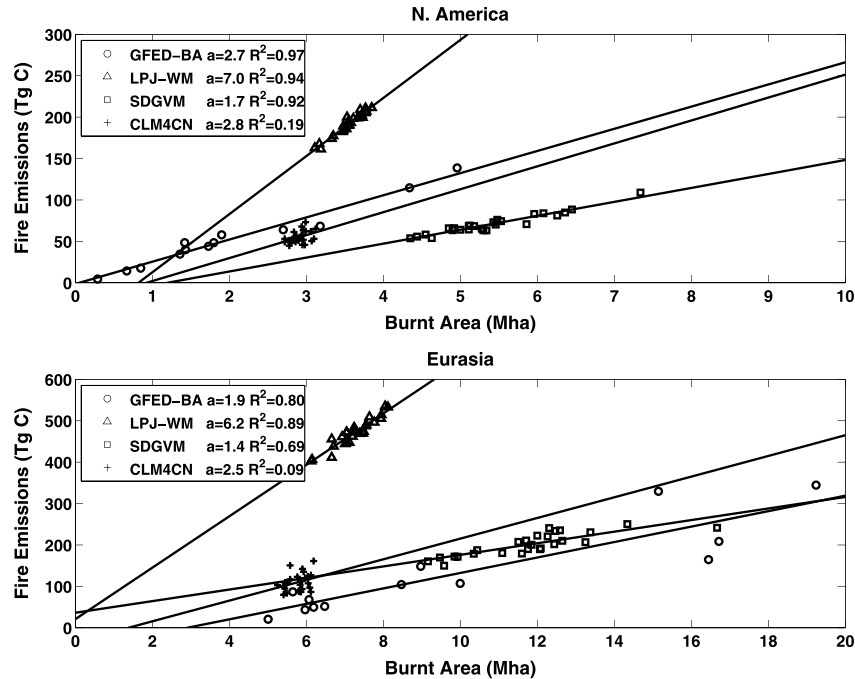


Figure 7. Regression of annual fire emissions (Tg C) against annual burned area (Mha) for the three DVMs (1981–2006) and GFED (1997–2009) over North America and Eurasia. The slope of the regression, a (Tg C/Mha), and the R^2 coefficient are given in the key.

Table 4. Definitions of Fuel Load and Combustion Completeness in the Three DVMs and in the CASA Model Used by GFED^a

	LPJ-WM	SDGVM	CLM4CN	GFED (CASA)
Fuel load	AGB, BGB, and litter	AGB only	AGB, BGB, and litter	AGB, BGB, and litter
Combustion completeness	Biomass: 100% Litter: 100%	AGB: 80%	Leaves and fine roots: 100% Stem and coarse roots: 20% Litter: 100% Woody debris: 40%	Leaves: 80–100% Stems: 20–40% Fine litter: 90–100% Woody debris: 40–60% Litter: 100%

^aAGB and BGB refer to aboveground and belowground biomass, respectively.

4. Discussion

[45] Two questions immediately arise from the results in section 3:

[46] 1. What is the explanation for the large differences between different estimates of fire emissions, and are there data to help clarify which model best represents the fire process?

[47] 2. Do the striking differences between the statistical properties of observed and modeled burned areas have consequences for other properties of the system, such as NBP and biomass?

4.1. Differences Between Model Parameterizations of Fire Emissions and Their Consequences

[48] The different model estimates of carbon emissions seen in section 3.3 do not stem from fundamental differences between the models, since they all use an approach that weights the area burned by the available fuel load while factoring in variables that define the combustion process. However, the models make different assumptions about the fuel load and combustion completeness (defined as the fraction of burnt fuel that is emitted to the atmosphere), as summarized in Table 4. In addition, the models assign a fire mortality factor to each PFT, which defines the fraction of individuals in the burned area that will be affected by fire. LPJ-WM and CLM4CN assign similar values to this factor for each of the tree PFTs and the value of 1 for herbaceous cover, while SDGVM assigns the value of 1 to all PFTs.

[49] SDGVM treats only aboveground biomass as fuel, whereas LPJ-WM and CLM4CN include belowground biomass and litter. Hence, SDGVM has a much smaller fuel load and yields much lower carbon emissions, despite burning around 60–100% more area (see Table 3 and Figure 7). LPJ-WM and CLM4CN produce similar burned areas, but LPJ-WM yields carbon emissions that are more than 4 times greater. A major factor in this discrepancy comes from burning of litter, which accounts for 56% of the emissions (372 Tg C yr⁻¹) in LPJ-WM but only 30% (50 Tg C yr⁻¹) in CLM4CN. This large difference arises partly from the much larger litter pool in LPJ-WM (an average value of 103 Pg C compared with 21 Pg C for CLM4CN); LPJ-WM also treats litter as a single pool with a combustion completeness of 100%, while CLM4CN assigns different values of combustion completeness to coarse woody debris, leaf litter, etc. In particular, in CLM4CN, the litter mainly consists of coarse woody debris, for which the combustion completeness is only 40%.

[50] Emissions from biomass burning are also larger in LPJ-WM than CLM4CN (average values of 290 Tg C yr⁻¹ and 114 Tg C yr⁻¹, respectively). This arises partly from LPJ-WM having 9.27×10^4 Tg C of biomass compared to 7.47×10^4 Tg C in CLM4CN, but more important is that

LPJ-WM assumes complete combustion of aboveground and belowground biomass, while CLM4CN completely burns the leaves and fine roots but assigns a combustion completeness factor of only 20% to the stem and coarse roots [Oleson *et al.*, 2010]. Note that the more complex CLM4CN scheme is similar to that adopted by CASA; hence, the large differences between them (Figure 7) reflect the very low variability in burned area in CLM4CN, together with differences in the carbon pools estimated in the models. However, we do not have access to the details of the CASA carbon calculations underlying the GFED estimates and hence cannot provide quantitative assessment of these differences.

[51] Overall, it is clear that the models disagree markedly about the relative importance of emissions from litter and from biomass: LPJ-WM produces 28% more emissions from litter than biomass, CLM4CN produces 66% less, while the whole of the 272 Tg C yr⁻¹ emitted by fire from SDGVM comes from burning aboveground biomass. This immediately raises the question of whether there are empirical data on the combustion completeness of carbon pools in northern high latitudes that can be used to test the models.

[52] As noted by *van der Werf et al.* [2010], the accuracy of fire emission estimates is limited by the available information on combustion completeness and emission factors, which is sparse and unsystematic and typically refers to specific fire events [Mack *et al.*, 2011] or experimental fires [FIRESCAN, 1996]. The available studies show that consumption of both biomass and litter by fire varies greatly, depending on environmental factors, the types of fire, and the type of ecosystem. Several investigators have parameterized combustion completeness according to fire severity and fire type. For example, in *Conard and Ivanova* [1997], the combustion completeness values for both understory vegetation and litter are taken to be 100% in high-severity canopy fires; 90% and 50%, respectively, for high-severity surface fires; and 50% and 10%, respectively, for low-severity surface fires. About 15% of the woody biomass is consumed in canopy fires, but this concerned a specific tree species. *Soja et al.* [2004] reported typical values of soil organic matter consumed by high-, medium-, and low-severity fires as 5, 2, and 1 cm in a standard scenario and 10, 4, and 2 cm in an extreme scenario.

[53] Although sparse, these observations suggest that the more complete parameterization of fuel load in CLM4CN is likely to be more realistic. However, the data also indicate that combustion completeness and fire severity are not independent, as assumed by the DVMs (though not by CASA, in which combustion completeness is proportional to soil moisture, which is used as a proxy of fire severity). In recognition of this, *Thonicke et al.* [2010] released an improved version of the LPJ model which used a new fire model (SPITFIRE) that linked fire severity to litter combustion completeness.

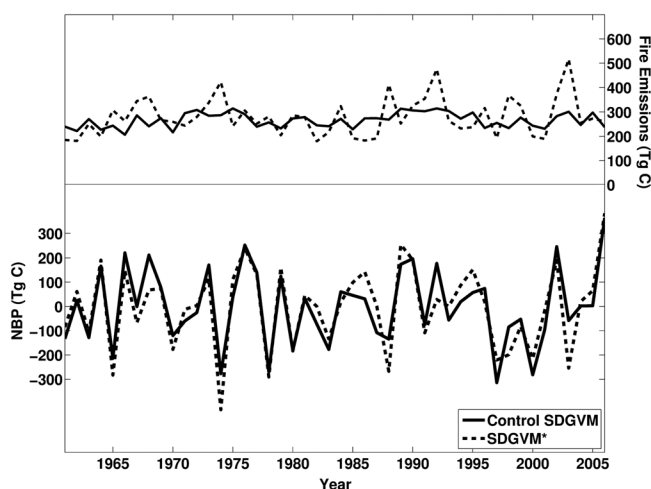


Figure 8. Time series (1960–2006) of the detrended (bottom, left axis) NBP and (top, right axis) fire emissions for SDGVM (solid lines) and its modified version, SDGVM* (dashed lines).

However, this still underestimated the interannual variability of burned area in the boreal zone, indicating that steps are still needed to represent more accurately the stochastic nature of fires. In addition, this version of the model does not include organic soils, boreal PFTs, or permafrost, unlike LPJ-WM, so it was not appropriate for this study.

4.2. The Effects of Improving the Spatiotemporal Description of Burned Area on Model Estimates of High-Latitude Processes

[54] Section 2.3 described modifications to SDGVM and LPJ-WM that make the statistical properties of their estimates of burned area conform more closely to observations. The need to consider modifications to both models stems from the suitability of each model for the issues addressed below. SDGVM has a particularly simple relation between fire and emissions, so it is well suited to investigating the role of fire in the interannual variability of NBP. Unlike SDGVM, LPJ-WM incorporates permafrost dynamics, so it is suitable for investigating fire-permafrost links.

4.2.1. The Effects of Enhanced Interannual Variability of Burned Area on NBP and Biomass

[55] Increasing the variability in burned area to be consistent with observations (see section 2.3.1) causes an increase from 30 Tg yr^{-1} to 79 Tg yr^{-1} in the interannual variability of the fire emissions calculated by SDGVM over the period 1960–2006. There is an associated increase in the interannual variability of NBP, but only by 15%, and it is still dominated by climate variability. Only 22% of the adjusted NBP variance can be attributed to the variance of the adjusted fire emissions, and there is little correlation between NBP and the size of the emissions (see Figure 8). These model-based results imply that fire/nonfire years are not the main determinant of whether a given year will be a CO_2 sink or a source, and fire emissions are not the major driver of the observed variability of land-atmosphere carbon exchange. A similar conclusion would be drawn for CLM4CN and GFED, because both have significantly smaller total fire emissions than SDGVM (see Table 2). This is consistent with the finding of *Prentice et al.* [2011], also model based, that the CO_2 fluxes produced by GFED during 1997–2005 would have

contributed only a third of the variability in total global CO_2 flux inferred from atmospheric inversion, despite earlier studies postulating that biomass burning is the major component in land-atmosphere carbon flux anomalies [*Nevison et al.*, 2008; *Patra et al.*, 2005]. Nevertheless, our conclusion relies on the model used to calculate fire emissions and may have been different for the much higher values from LPJ-WM; we did not pursue this as these are probably too high (see Figure 6). This emphasizes the need for more direct measurements of emissions, as such are increasingly becoming available from measurements of Fire Radiative Power [*Kaiser et al.*, 2012].

[56] The effects on biomass are illustrated for the panboreal region in Figure 9, which shows the difference between SDGVM and SDGVM* as a percentage of the unmodified value. Although the overall effect is to slightly reduce overall biomass, the modified fire regime leads to a complex pattern of increases and decreases in the local mean biomass, essentially because it causes the occurrence of very large fires destroying large parts of the vegetation in many grid cells in some years, thus altering the age structure in the forest component of vegetation. This pattern of heterogeneity varies though time, but its statistical properties are stable and does not give rise to major changes in the mean NBP.

4.2.2. The Effects of Modified Burned Area Statistics on Permafrost

[57] In a boreal Alaskan forest underlain by permafrost, *Dyrness et al.* [1986] found that the active layer depth increased by 40–140 cm 7 years after fire, and this effect can continue for 20–30 years [*Viereck*, 1983]. The effects of fire on permafrost are also related to fire severity [*Brown*, 1983]. Neither of these aspects of the observations can be simulated for the current fire parameterizations in models, under which no more than 5% of any given grid cell is burnt (see Figure 5). Since the effects of disturbance are averaged across each grid cell, insufficient litter and vegetation are removed to disrupt the thermal balance of the soil column within the grid cell and cause the breakdown of permafrost. In other words, current model formulations cannot represent the disturbance to permafrost, because fires destroying large parts of the vegetation and litter in a grid cell never occur in the models.

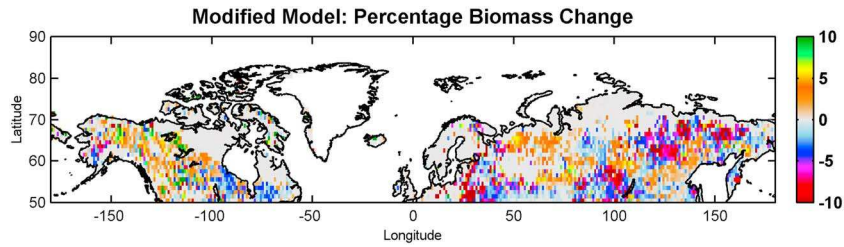


Figure 9. Percentage difference in biomass between modified and unmodified SDGVM calculations, i.e., $100 \times (\text{SDGVM}^* - \text{SDGVM})/\text{SDGVM}$, averaged over 1997–2006.

[58] The modification to LPJ-WM described in section 2.3.2 changes this situation by allowing large fractions of some grid cells to burn. Since 100% of the insulating litter layer is removed in the burned fraction (see Table 4), this has significant effects on soil temperature and hence on permafrost. Furthermore, removal of canopy by fire alters the radiation budget: for example, prior to disturbance, 30–65% of incoming solar radiation reaches the forest floor in black spruce forests [Slaughter, 1983], while after a fire, it exceeds 90% [Kasischke *et al.*, 1995]. This cannot be simulated by the current version of LPJ-WM, which lacks a full radiation balance in its energy calculations. Hence, a rough approximation was made in which the input air temperature, which acts as an upper boundary condition for the heat diffusion equation, was increased in the year after a fire and decreased as an exponential function of tree cover. This simulates an increase of leaf area index and associated attenuation of radiation according to Beer-Lambert’s law.

[59] The cumulative effect of these two modifications is illustrated by Figure 10, in which the upper plot shows the monthly soil temperatures at a depth of 10 cm calculated by LPJ-WMa at a location dominated by deciduous needle-leaved forest in northern Siberia after a fire with 99% fraction

of burn. Following the disturbance, the model initially sets herbaceous cover as the dominant PFT in the grid cell, while the needle-leaved PFT becomes dominant after 15 years. Figure 10 shows that the removal of litter and its subsequent damping effect increases the monthly variability of soil temperature as it becomes more susceptible to air temperature and its periodic fluctuations. Since summer soil temperatures now exceed 0°C, summer thaw depth increases by over 1.0 m and requires more than 60 years to return to its predisturbed value. These values are closer to field measurements than when the boundary conditions were unchanged, in which case the increase in maximum thaw depth due to loss of litter is less than 0.5 m, although the time to recovery of the original temperature conditions is the same (see Figure 10).

[60] Although the modifications to LPJ-WM provide more realistic simulations of permafrost dynamics following a fire by generating greater thaw depths, the current model formulation cannot capture the full extent of fire-permafrost interactions, e.g., thaw depth increases for several years after a fire, not just in the immediately following year [MacKay, 1970; Yoshikawa *et al.*, 2002]. Achieving this is hindered by the fact that fire is not treated as a continuous process in the model; instead, all the burn effects, e.g., loss of canopy

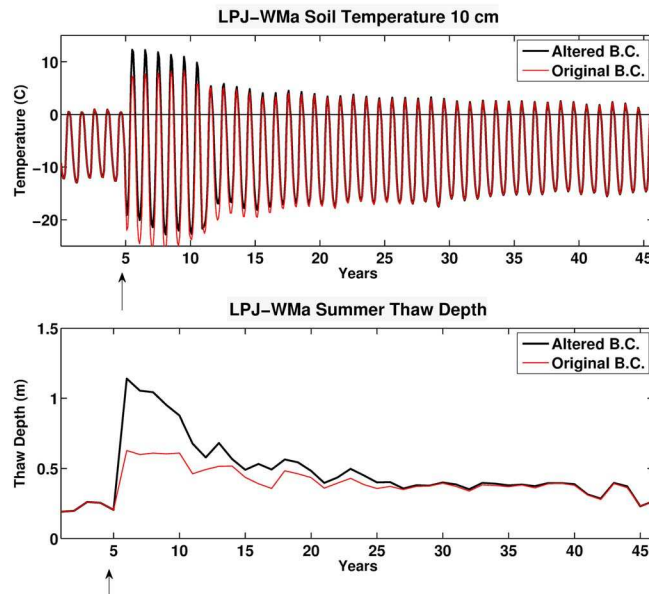


Figure 10. (top) Monthly soil temperatures for altered and original boundary conditions (B.C.) at a depth of 0.1 m produced by LPJ-WMa at a site which experienced more than 99% of burn; the arrow marks the year of the fire disturbance. (bottom) Thaw depth averaged over summer months for the same site. The arrow indicates fire event.

and litter, are imposed on January 1 of each year. Hence, the expected thawing of permafrost after a summer fire is not properly represented. Clearly, the radiation balance also needs to be treated properly, rather than in the ad hoc approach used here to illustrate its importance. Furthermore, the effects of localized intense fire events that occupy only a small part of a grid cell are not properly represented because of the averaging across grid cells used by models, even though these subgrid cell events are likely to form an important driver of the dynamics of permafrost.

5. Conclusions

[61] Fire is an endemic process at high latitudes, connected to a range of other land surface properties, such as land cover, biomass, and permafrost, and intimately linked to the carbon balance of the high-latitude land surface. Much of our current understanding of these links and their climate consequences is through land surface models, so it is essential to ensure that the process representations and parameterizations in these models are consistent with observations; only then will they be able to provide trustworthy predictions for a changing climate. Over the vast panboreal region, a key source of information on fire is satellite data. Comparisons between satellite-based burned area data from the Global Fire Emissions Database (GFED) and three DVMs (LPJ-WM, CLM4CN, and SDGVM) indicate that all models fail to represent the observed spatial and temporal properties of the fire regime and that there are large discrepancies between models and data with regard to average annual burned area. Although the three DVMs give comparable values of the boreal net biome production (NBP), fire emissions are found to differ by a factor 4 between the models, because of widely different estimates of burned area and because of different parameterizations of the fuel load and combustion process. Including a more realistic representation of the fire regime in the models shows that for northern high latitudes, (i) severe fire years do not coincide with CO₂ source years or vice versa; (ii) increasing the interannual variability of burned area to be consistent with data increases the interannual variability of NBP, but climate variability remains the main factor determining its magnitude; and (iii) overall biomass values alter only slightly, but the spatial distribution of biomass exhibits changes. It must be stressed that these conclusions are derived using model estimates of fire emissions, which this study has demonstrated to be problematic; thus, they should not be considered robust until verified by measurements or by models with considerably improved representation of boreal fire processes. We also demonstrate that it is crucial to alter the current representations of fire occurrence and severity in land surface models if the links between permafrost and fire are to be captured, in particular, the dynamics of permafrost properties, such as active layer depth. This is especially important if models are to be used to predict the effects of a changing climate, because of the consequences of permafrost changes for greenhouse gas emissions, hydrology, and land cover.

[62] This study highlights two areas where further work is clearly needed. The first is improved experimental data on fire processes at high latitudes, with regard to the pools entrained in fire events and the combustion completeness of these pools. Lack of knowledge about these factors is a major source of uncertainty in model estimates, both in the DVMs

and in GFED (through CASA). This is not a fundamental weakness of the models, only of the parameter settings within their representations of fire, particularly for CLM4CN and CASA, which already contain a comprehensive description of the pools contributing to the fuel load.

[63] However, there are fundamental limitations in the current ways that fire occurrence and fire severity are represented in the models, with follow-on consequences for the need for better energy balance representations if models are to be capable of predicting permafrost dynamics and associated effects on greenhouse gas emissions, hydrology, and land cover. Removing these limitations constitutes the second major area where further work is needed. This has two components:

[64] 1. Models for fire occurrence and severity that more realistically capture the observed high variability in space and time of high-latitude fires are formulated. A purely statistical approach has been used in this paper to assess the importance of representing such variability; its most significant effect, within the limits of our study, appears to be on permafrost. However, for predictive purposes under changing climate, a more mechanistic approach may be preferable, with a stochastic component related to ignition probabilities. An associated issue is that most current models simply average fire-affected areas back into the overall vegetation structure in a grid cell, which dilutes their effect. Internal grid cell heterogeneity is required if the effects of smaller severe fires on vegetation and soil dynamics are to be correctly represented.

[65] 2. More complete models for energy balance after fire are needed to include the effects of both heat diffusion and radiation. Failure to include the latter leads to errors in the predicted mean soil temperature and to large underestimates of the time for permafrost to recover after fire. This may also require better representations of vegetation, for example, to include the thermal consequences of a moss layer.

[66] **Acknowledgments.** This study was carried out as part of European Union FP7-SPACE-2009-1 Collaborative Project 242446, MONARCH-A: Monitoring and assessing regional climate change in high latitudes and the Arctic. The authors would like to thank the partners of the TRENDY project for data access to model runs. We would also like to thank Rita Wania for access to the code and technical assistance on the LPJ-WM model.

References

- Arino, O., S. Casadio, and D. Serpe (2012), Global night-time fire season timing and fire count trends using the ATSR instrument series, *Remote Sens. Environ.*, *116*, 226–238, doi:10.1016/j.rse.2011.05.025.
- Baker, D. F., et al. (2006), TransCom 3 inversion intercomparison: Impact of transport model errors on the interannual variability of regional CO₂ fluxes, 1988–2003, *Global Biogeochem. Cycles*, *20*, GB1002, doi:10.1029/2004gb002439.
- Bowman, D. M. J. S., et al. (2009), Fire in the Earth system, *Science*, *324*(5926), 481–484, doi:10.1126/science.1163886.
- Brown, R. J. E. (1983), Effects of fire on permafrost ground thermal regime, in *The Role of Fire in Northern Circumpolar Ecosystems*, edited by R. W. Wein and D. A. MacLean, pp. 97–110, John Wiley, New York.
- Christensen, J. H., B. Hewitson, A. Busuioc, A. Chen, X. Gao, I. Held, R. Jones, and R. K. Kolli (2007), Regional Climate Projections, in *Climate Change 2007: The Physical Science Basis. Contribution of Working Group I to the Fourth Assessment Report of the Intergovernmental Panel on Climate Change*, edited by S. Solomon, et al., pp. 847–940, Cambridge University Press, Cambridge, U.K.
- Collins, W. D., et al. (2006), The Community Climate System Model version 3 (CCSM3), *J. Clim.*, *19*(11), 2122–2143.
- Conard, S. G., and G. A. Ivanova (1997), Wildfire in Russian boreal forests—Potential impacts of fire regime characteristics on emissions and global carbon balance estimates, *Environ. Pollut.*, *98*(3), 305–313.

- Corell, R. (2005), Arctic climate impact assessment, *Bull. Am. Meteorol. Soc.*, 86(6), 860–861.
- Cox, P., and D. Stephenson (2007), Climate change—A changing climate for prediction, *Science*, 317(5835), 207–208, doi:10.1126/science.1145956.
- Cramer, W., et al. (2001), Global response of terrestrial ecosystem structure and function to CO₂ and climate change: Results from six dynamic global vegetation models, *Global Change Biol.*, 7(4), 357–373.
- Dymess, C. T., L. A. Viereck, and K. Van Kleeve (1986), Fire in taiga communities of interior Alaska, in *Ecological Series: Forest Ecosystems in the Alaskan Taiga*, edited by K. Van Kleeve, pp. 74–86, Springer, New York.
- FIRESCAN (1996), Fire Research Campaign Asia-North, in *Biomass Burning and Global Change*, edited by J. S. Levine, pp. 848–873, MIT Press, Cambridge, Mass.
- Flannigan, M. D., and C. E. Van Wagner (1991), Climate change and wildfire in Canada, *Can. J. For. Res.*, 21(1), 66–72, doi:10.1139/X91-010.
- Friedlingstein, P., et al. (2006), Climate-carbon cycle feedback analysis: Results from the C(4)MIP model intercomparison, *J. Clim.*, 19(14), 3337–3353.
- GCOS (2004), *Implementation Plan for the Global Observing System for Climate in Support of the UNFCCC*, GCOS-92, WMO Technical Document No. 1219WMO, Geneva, Switzerland.
- GCOS (2010), *Implementation Plan for the Global Observing System for Climate in Support of the UNFCCC (2010 Update)*, WMO, Geneva.
- Gerten, D., S. Schaphoff, U. Haberlandt, W. Lucht, and S. Sitch (2004), Terrestrial vegetation and water balance—Hydrological evaluation of a dynamic global vegetation model, *J. Hydrol.*, 286(1–4), 249–270, doi:10.1016/j.jhydrol.2003.09.029.
- Giglio, L. (2010), *MODIS Collection 5 Active Fire Product User's Guide, Version 2.4*, Department of Geography, University of Maryland, Md.
- Giglio, L., J. T. Randerson, G. R. van der Werf, P. S. Kasibhatla, G. J. Collatz, D. C. Morton, and R. S. DeFries (2010), Assessing variability and long-term trends in burned area by merging multiple satellite fire products, *Biogeosciences*, 7(3), 1171–1186.
- Gurney, K. R., et al. (2003), TransCom 3 CO₂ inversion intercomparison: 1. Annual mean control results and sensitivity to transport and prior flux information, *Tellus, Ser. B*, 55(2), 555–579.
- Jiang, Y., Q. Zhuang, and D. Mandallaz (2012), Modeling large fire frequency and burned area in Canadian terrestrial ecosystems with Poisson models, *Environ. Model. Assess.*, 17, 483–493, doi:10.1007/s10666-012-9307-5.
- Kaiser, J. W., et al. (2012), Biomass burning emissions estimated with a global fire assimilation system based on observed fire radiative power, *Biogeosciences*, 9(1), 527–554, doi:10.5194/bg-9-527-2012.
- Kanamitsu, M., W. Ebisuzaki, J. Woollen, S. K. Yang, J. J. Hnilo, M. Fiorino, and G. L. Potter (2002), Ncep-Doe Amip-Ii Reanalysis (R-2), *Bull. Am. Meteorol. Soc.*, 83(11), 1631–1643, doi:10.1175/Bams-83-11-1631.
- Kasischke, E. S., N. L. Christensen, and B. J. Stocks (1995), Fire, global warming, and the carbon balance of boreal forests, *Ecol. Appl.*, 5(2), 437–451.
- Kloster, S., N. M. Mahowald, J. T. Randerson, P. E. Thornton, F. M. Hoffman, S. Levis, P. J. Lawrence, J. J. Feddema, K. W. Oleson, and D. M. Lawrence (2010), Fire dynamics during the 20th century simulated by the Community Land Model, *Biogeosciences*, 7(6), 1877–1902, doi:10.5194/bg-7-1877-2010.
- Lawrence, D. M., and A. G. Slater (2008), Incorporating organic soil into a global climate model, *Clim. Dyn.*, 30(2–3), 145–160, doi:10.1007/s00382-007-0278-1.
- Lawrence, D. M., A. G. Slater, V. E. Romanovsky, and D. J. Nicolsky (2008), Sensitivity of a model projection of near-surface permafrost degradation to soil column depth and representation of soil organic matter, *J. Geophys. Res.*, 113, F02011, doi:10.1029/2007jg000883.
- Lawrence, D. M., et al. (2011), Parameterization improvements and functional and structural advances in Version 4 of the Community Land Model, *J. Adv. Model. Earth Syst.*, 3, M03001, doi:10.1029/2011ms000045.
- Le Quere, C., et al. (2009), Trends in the sources and sinks of carbon dioxide, *Nat. Geosci.*, 2(12), 831–836, doi:10.1038/ngeo689.
- Mack, M. C., M. S. Bret-Harte, T. N. Hollingsworth, R. R. Jandt, E. A. G. Schuur, G. R. Shaver, and D. L. Verbyla (2011), Carbon loss from an unprecedented Arctic tundra wildfire, *Nature*, 475(7357), 489–492, doi:10.1038/nature10283.
- MacKay, J. R. (1970), Disturbances to the tundra and forest tundra environments of the western Arctic, *Can. Geotech. J.*, 7(4), 420–432.
- Mandallaz, D., and R. Ye (1997), Prediction of forest fires with Poisson models, *Can. J. For. Res.*, 27(10), 1685–1694.
- McGuire, A. D., J. M. Melillo, D. W. Kicklighter, and L. A. Joyce (1995), Equilibrium responses of soil carbon to climate change: Empirical and process-based estimates, *J. Biogeogr.*, 22(4–5), 785–796.
- McGuire, A. D., L. G. Anderson, T. R. Christensen, S. Dallimore, L. D. Guo, D. J. Hayes, M. Heimann, T. D. Lorenson, R. W. Macdonald, and N. Roulet (2009), Sensitivity of the carbon cycle in the Arctic to climate change, *Ecol. Monogr.*, 79(4), 523–555.
- Mitchell, T. D., and P. D. Jones (2005), An improved method of constructing a database of monthly climate observations and associated high-resolution grids, *Int. J. Climatol.*, 25(6), 693–712, doi:10.1002/joc.1181.
- Nevison, C. D., N. M. Mahowald, S. C. Doney, I. D. Lima, G. R. Van der Werf, J. T. Randerson, D. F. Baker, P. Kasibhatla, and G. A. McKinley (2008), Contribution of ocean, fossil fuel, land biosphere, and biomass burning carbon fluxes to seasonal and interannual variability in atmospheric CO₂, *J. Geophys. Res.*, 113, G01010, doi:10.1029/2007JG000408.
- Oleson, K. W., et al. (2010), *Technical Description of Version 4.0 of the Community Land Model*, NCAR Technical Note 47, 257 pp. Boulder, Colo. NCAR.
- Patra, P. K., M. Ishizawa, S. Maksyutov, T. Nakazawa, and G. Inoue (2005), Role of biomass burning and climate anomalies for land-atmosphere carbon fluxes based on inverse modeling of atmospheric CO₂, *Global Biogeochem. Cycles*, 19, GB3005, doi:10.1029/2004gb002258.
- Pechony, O., and D. T. Shindell (2010), Driving forces of global wildfires over the past millennium and the forthcoming century, *Proc. Natl. Acad. Sci. U. S. A.*, 107(45), 19,167–19,170, doi:10.1073/pnas.1003669107.
- Piao, S. L., J. Y. Fang, P. Ciais, P. Peylin, Y. Huang, S. Sitch, and T. Wang (2009), The carbon balance of terrestrial ecosystems in China, *Nature*, 458(7241), 1009–1013, doi:10.1038/Nature07944.
- Potter, C. S., J. T. Randerson, C. B. Field, P. A. Matson, P. M. Vitousek, H. A. Mooney, and S. A. Klooster (1993), Terrestrial ecosystem production—A process model based on global satellite and surface data, *Global Biogeochem. Cycles*, 7(4), 811–841.
- Prentice, I. C., D. I. Kelley, P. N. Foster, P. Friedlingstein, S. P. Harrison, and P. J. Bartlein (2011), Modeling fire and the terrestrial carbon balance, *Global Biogeochem. Cycles*, 25, GB3005, doi:10.1029/2010gb003906.
- Quegan, S., C. Beer, A. Shvidenko, I. McCallum, I. C. Handoh, P. Peylin, C. Rodenbeck, W. Lucht, S. Nilsson, and C. Schmulius (2011), Estimating the carbon balance of central Siberia using a landscape-ecosystem approach, atmospheric inversion and Dynamic Global Vegetation Models, *Global Change Biol.*, 17(1), 351–365, doi:10.1111/j.1365-2486.2010.02275.x.
- Roberts, G. J., and M. J. Wooster (2008), Fire detection and fire characterization over Africa using Meteosat SEVIRI, *IEEE Trans. Geosci. Remote Sens.*, 46(4), 1200–1218, doi:10.1109/Tgrs.2008.915751.
- Rödenbeck, C., S. Houweling, M. Gloor, and M. Heimann (2003), CO₂ flux history 1982–2001 inferred from atmospheric data using a global inversion of atmospheric transport, *Atmos. Chem. Phys.*, 3, 1919–1964.
- Roy, D. P., L. Boschetti, C. O. Justice, and J. Ju (2008), The collection 5 MODIS burned area product—Global evaluation by comparison with the MODIS active fire product, *Remote Sens. Environ.*, 112(9), 3690–3707, doi:10.1016/j.rse.2008.05.013.
- Serreze, M. C., and J. A. Francis (2006), The arctic amplification debate, *Clim. Change*, 76(3–4), 241–264, doi:10.1007/s10584-005-9017-y.
- Sitch, S., et al. (2003), Evaluation of ecosystem dynamics, plant geography and terrestrial carbon cycling in the LPJ dynamic global vegetation model, *Global Change Biol.*, 9(2), 161–185.
- Slaughter, C. W. (1983), Summer shortwave radiation at a subarctic forest site, *Can. J. For. Res.*, 13(5), 740–746.
- Soja, A. J., W. R. Cofer, H. H. Shugart, A. I. Sukhinin, P. W. Stackhouse, D. J. McRae, and S. G. Conard (2004), Estimating fire emissions and disparities in boreal Siberia (1998–2002), *J. Geophys. Res.*, 109, D14S06, doi:10.1029/2004jd004570.
- Stocks, B. J., et al. (1998), Climate change and forest fire potential in Russian and Canadian boreal forests, *Clim. Change*, 38(1), 1–13.
- Stocks, B. J., et al. (2002), Large forest fires in Canada, 1959–1997, *J. Geophys. Res.*, 108(D1), 8149, doi:10.1029/2001JD000484.
- Street, L. E., P. C. Stoy, M. Sommerkorn, B. J. Fletcher, V. L. Sloan, T. C. Hill, and M. Williams (2012), Seasonal bryophyte productivity in the sub-Arctic: A comparison with vascular plants, *Funct. Ecol.*, 26(2), 365–378, doi:10.1111/j.1365-2435.2011.01954.x.
- Tarnocai, C., J. G. Canadell, E. A. G. Schuur, P. Kuhry, G. Mazhitova, and S. Zimov (2009), Soil organic carbon pools in the northern circumpolar permafrost region, *Global Biogeochem. Cycles*, 23, GB2023, doi:10.1029/2008gb003327.
- Thonicke, K., S. Venevsky, S. Sitch, and W. Cramer (2001), The role of fire disturbance for global vegetation dynamics: Coupling fire into a Dynamic Global Vegetation Model, *Global. Ecol. Biogeogr.*, 10(6), 661–677.
- Thonicke, K., A. Spessa, I. C. Prentice, S. P. Harrison, L. Dong, and C. Carmona-Moreno (2010), The influence of vegetation, fire spread and fire behaviour on biomass burning and trace gas emissions: Results from a process-based model, *Biogeosciences*, 7(6), 1991–2011, doi:10.5194/bg-7-1991-2010.
- Thornton, P. E., J. F. Lamarque, N. A. Rosenbloom, and N. M. Mahowald (2007), Influence of carbon-nitrogen cycle coupling on land model response to CO₂ fertilization and climate variability, *Global Biogeochem. Cycles*, 21, GB4018, doi:10.1029/2006gb002868.

- Tjiputra, J. F., K. Assmann, M. Bentsen, I. Bethke, O. H. Ottera, C. Sturm, and C. Heinze (2010), Bergen Earth system model (BCM-C): Model description and regional climate-carbon cycle feedbacks assessment, *Geosci. Model Dev.*, 3(1), 123–141.
- Turetsky, M., K. Wieder, L. Halsey, and D. Vitt (2002), Current disturbance and the diminishing peatland carbon sink, *Geophys. Res. Lett.*, 29(11), 1526, doi:10.1029/2001gl014000.
- Viereck, L. A. (1983), The effects of fire in black spruce ecosystems of Alaska and northern Canada, in *The Role of Fire in Northern Circumpolar Ecosystems*, edited by R. W. Wien and D. A. MacLean, pp. 201–220, Wiley & Sons Ltd, Chichester, UK.
- Wania, R., I. Ross, and I. C. Prentice (2009), Integrating peatlands and permafrost into a dynamic global vegetation model: 1. Evaluation and sensitivity of physical land surface processes, *Global Biogeochem. Cycles*, 23, GB3014, doi:10.1029/2008gb003412.
- van der Werf, G. R., J. T. Randerson, L. Giglio, G. J. Collatz, P. S. Kasibhatla, and A. F. Arellano (2006), Interannual variability in global biomass burning emissions from 1997 to 2004, *Atmos. Chem. Phys.*, 6, 3423–3441.
- van der Werf, G. R., J. T. Randerson, L. Giglio, G. J. Collatz, M. Mu, P. S. Kasibhatla, D. C. Morton, R. S. DeFries, Y. Jin, and T. T. van Leeuwen (2010), Global fire emissions and the contribution of deforestation, savanna, forest, agricultural, and peat fires (1997–2009), *Atmos. Chem. Phys.*, 10(23), 11,707–11,735, doi:10.5194/acp-10-11707-2010.
- Woodward, F. I., and M. R. Lomas (2004), Vegetation dynamics—simulating responses to climatic change, *Biol. Rev.*, 79(3), 643–670, doi:10.1017/S1464793103006419.
- Woodward, F. I., T. M. Smith, and W. R. Emanuel (1995), A Global land primary productivity and phytogeography model, *Global Biogeochem. Cycles*, 9(4), 471–490.
- Wooster, M. J., and Y. H. Zhang (2004), Boreal forest fires burn less intensely in Russia than in North America, *Geophys. Res. Lett.*, 31, L20505, doi:10.1029/2004GL020805.
- Wooster, M. J., G. Roberts, G. L. W. Perry, and Y. J. Kaufman (2005), Retrieval of biomass combustion rates and totals from fire radiative power observations: FRP derivation and calibration relationships between biomass consumption and fire radiative energy release, *J. Geophys. Res.*, 110, D24311, doi:10.1029/2005jd006318.
- Wotton, B. M., and M. D. Flannigan (1993), Length of the fire season in a changing climate, *For. Chron.*, 69(2), 187–192.
- Yoshikawa, K., W. R. Bolton, V. E. Romanovsky, M. Fukuda, and L. D. Hinzman (2002), Impacts of wildfire on the permafrost in the boreal forests of Interior Alaska, *J. Geophys. Res.*, 108(D1), 8148, doi:10.1029/2001jd000438.